Title
Dynamics of Mechanically Coupled Hair-Cell Bundles of the Inner Ear

Journal
Biophysical Journal, 120(2)

ISSN
0006-3495

Authors
Roongthumskul, Yuttana
Faber, Justin
Bozovic, Dolores

Publication Date
2021

DOI
10.1016/j.bpj.2020.11.2273

Peer reviewed

Biophysical Journal
Article

Biophysical Society

Dynamics of Mechanically Coupled Hair-Cell Bundles of the Inner Ear

Yuttana Roongthumskul,[1] Justin Faber,[2] and Dolores Bozovic[2,3,*]
[1]Department of Physics, Faculty of Science, Chulalongkorn University, Bangkok, Thailand; [2]Department of Physics & Astronomy, University of California, Los Angeles, Los Angeles, California; and [3]California NanoSystems Institute, University of California, Los Angeles, Los Angeles, California

ABSTRACT The high sensitivity and effective frequency discrimination of sound detection performed by the auditory system rely on the dynamics of a system of hair cells. In the inner ear, these acoustic receptors are primarily attached to an overlying structure that provides mechanical coupling between the hair bundles. Although the dynamics of individual hair bundles has been extensively investigated, the influence of mechanical coupling on the motility of the system of bundles remains underdetermined. We developed a technique of mechanically coupling two active hair bundles, enabling us to probe the dynamics of the coupled system experimentally. We demonstrated that the coupling could enhance the coherence of hair bundles' spontaneous oscillation, as well as their phase-locked response to sinusoidal stimuli, at the calcium concentration in the surrounding fluid near the physiological level. The empirical data were consistent with numerical results from a model of two coupled nonisochronous oscillators, each displaying a supercritical Hopf bifurcation. The model revealed that a weak coupling can poise the system of unstable oscillators closer to the bifurcation by a shift in the critical point. In addition, the dynamics of strongly coupled oscillators far from criticality suggested that individual hair bundles may be regarded as nonisochronous oscillators. An optimal degree of nonisochronicity was required for the observed tuning behavior in the coherence of autonomous motion of the coupled system.

SIGNIFICANCE Hair cells of the inner ear transduce acoustic energy into electrical signals via a deflection of hair bundles. Unlike a passive mechanical antenna, a free-standing hair bundle behaves as an active oscillator that can sustain autonomous oscillations as well as amplify a low-level stimulus. Hair bundles under physiological conditions are elastically coupled to each other via an extracellular matrix. Therefore, the dynamics of coupled nonlinear oscillators underlies the performance of the peripheral auditory system. Despite extensive theoretical investigations, there is limited experimental evidence that supports the significance of coupling on hair-bundle motility. We develop a technique to mechanically couple hair bundles and demonstrate the benefits of coupling on hair-bundle spontaneous motility.

INTRODUCTION

Signal transduction by the inner ear is performed by a system of hair cells. Owing to the nonlinearity and internal active processes of hair cells, the inner ear exhibits exquisite sensitivity and high frequency resolution (1,2). Under constant mechanical forces, the apical protrusion of a hair cell, called the hair bundle, displays a nonlinear force-displacement relationship because of the gating of the mechanosensitive transduction channels (3,4). The hair bundle under a sinusoidal driving force produces mechanical feedback that facilitates the amplification of low-level signals near a characteristic frequency (4–7). In nonmammalian species, active bundle motility likely constitutes the primary source of amplification. In the mammalian cochlea, a process termed electromotility, which refers to the hair cell's somatic length change upon variations in the membrane's potential (8), also influences the frequency selectivity as well as the amplitude threshold of hearing (9,10).

From a dynamical systems perspective, the sensitivity and frequency selectivity might be improved when a hair bundle operates near an instability. Hair-bundle motility can be described by a nonlinear oscillator near a bifurcation; at the critical point, the stability of the system switches from stationary to self-sustained oscillations. Under appropriate in vitro environments, undriven hair bundles robustly exhibit spontaneous oscillations (11), a behavior that corresponds to a

Submitted August 20, 2020, and accepted for publication November 30, 2020.

*Correspondence: bozovic@physics.ucla.edu

Editor: Padmini Rangamani.

https://doi.org/10.1016/j.bpj.2020.11.2273

limit-cycle oscillation of a dynamical system. Under different types of chemical and mechanical manipulations on hair bundles of in vitro preparations, these autonomous oscillations can be enhanced, attenuated, or suppressed, with the alterations in the amplitude and frequency consistent with a variety of bifurcations, including Hopf and saddle node on an invariant circle (12–14). In agreement with the theoretical predictions, individual hair bundles near a critical point have been experimentally demonstrated to display enhanced sensitivity and frequency selectivity to sinusoidal stimuli (15,16).

In addition to the dynamical state of individual hair bundles, mechanical coupling between hair bundles has been proposed as a mechanism that sharpens the frequency tuning and lowers the detection threshold of the inner ear (17–19). In the inner ear of most species, hair bundles are tightly anchored to an overlying extracellular matrix, such as the tectorial membrane in the mammalian cochlea or the otolithic membrane in the amphibian sacculus. This overlying structure provides strong coupling between neighboring bundles. Upon an increase in the bundles' separation, the coupling strength becomes progressively weaker. The performance of the inner ear epithelium thus relies on the dynamics of hair cells under various degrees of mechanical coupling.

The dynamics of coupled nonlinear oscillators have been extensively investigated because of their relevance in various fields of study (20,21). For the auditory system, several investigations suggest benefits of coupling on signal detection performed by groups of active, oscillatory hair bundles. Theoretical predictions reveal that a system of oscillating hair bundles with a large frequency dispersion may become quiescent under a sufficiently strong coupling, a phenomenon termed amplitude death (22,23). This regime shows a greatly enhanced signal/noise ratio in response to a driving force, making it an attractive alternative mechanism that the auditory system may utilize to achieve sensitivity in the presence of noise. Furthermore, coupling of unstable oscillators with a small difference in their characteristic frequencies reduces the effective noise level, resulting in more coherent autonomous oscillations as well as the enhanced quality factor in their response to a sinusoidal driving force (18,24–26). This has been experimentally demonstrated in a system of a small number of spontaneously oscillating hair bundles in a chemical environment that approximates the physiological conditions (27,28).

Although the stability of in vivo hair bundles remains unclear, an understanding of the role of mechanical coupling on the motility of hair bundles across different dynamical states would help establish the connection between the dynamics of one hair bundle and the response of the full auditory system. To elucidate this connection, we investigate the autonomous dynamics of coupled hair bundles, both experimentally and theoretically. First, we study a mathematical model of two mutually coupled nonisochronous oscillators, each displaying a supercritical Hopf bifurcation. The theoretical predictions in the strong-coupling limit are used to describe the activity of two mechanically coupled hair bundles from the bullfrog sacculus. The dynamical state of the individual bundles is manipulated across the critical point by increasing the level of calcium concentration of the artificial endolymph solution. Near the physiological calcium level, we observed two types of behavior of spontaneous dynamics as well as two types of response functions to sinusoidal forces of various frequencies. These two distinct behaviors correspond to two different degrees of nonisochronicity in the model of coupled oscillators. Finally, using a microscopic model of hair-bundle mechanics, we illustrate that a calcium-sensitive elastic element within the bundle could potentially contribute to the nonisochronicity.

MATERIALS AND METHODS

Mathematical model of two mutually coupled nonlinear oscillators

We described the dynamics of each hair bundle by the normal form of a nonlinear system near a supercritical Hopf bifurcation (Eqs. 1 and 2). The bundles' positions were represented by the real parts of the complex variables $z_1(t)$ and $z_2(t)$. The imaginary parts served as hidden variables, not accessible in the experimental recordings. Both oscillators had identical control parameters μ, which determined the dynamical state of the system.

In the absence of coupling, a single oscillator displays autonomous motion when $\mu > 0$ (Fig. 1 *A*). The trajectory of the oscillator in the complex phase plane, constructed from the real and imaginary part of the dynamical variable, $z(t)$, converges to a limit cycle. The oscillation amplitude is determined by the value of the control parameter, $R = \mu^{1/2}$. At $\mu = 0$, the system undergoes a supercritical Hopf bifurcation because this is the boundary between the oscillatory and the quiescent states. The oscillator remains at rest when $\mu < 0$, with its phase-space trajectory terminating at a stable fixed point.

The dynamics of individual hair bundles are typically modeled with the isochronous form of the Hopf oscillator, $\beta = 0$. An isochronous oscillator is one for which the frequency is independent of the amplitude, such as the simple harmonic oscillator. However, several experimental observations demonstrate the nonisochronous behavior of single hair bundles; the frequency of the autonomous oscillation depends on the amplitude. For a nonisochronous oscillator near a supercritical Hopf bifurcation, the oscillation frequency is determined by $\Omega = \omega_0 - \beta R^2$, where ω_0 denotes the characteristic frequency of the oscillator, with the value of β determining the degree of nonisochronicity of the oscillator (Fig. 1 *A*, *inset*, and Fig. 1 *B*). In this work, identical values of β were assigned to both oscillators for simplicity.

The coupling term was modeled to facilitate comparisons to the physiological data. In our experiments, sets of two hair bundles were connected by attachment to the same glass probe (Fig. 1, *C* and *D*). Because of the transverse motion of the probe, the coupling stiffness between bundles due to an elastic force was estimated by the bending stiffness of a thin rod whose length was equal to the bundle separation. The coupling constant was ~1 N/m, which significantly dominated the dissipative force (Supporting Materials and Methods, Section I). Note that the stiffness of the full coupling probe was neglected in the model because it was significantly more compliant than the portion attached to the bundles. The coupling term was thus modeled as an elastic element whose stiffness was real and denoted by K. Its extension was determined by the difference in the oscillators' displacements. We note that in our model, direct coupling was limited to the real component and did not involve the imaginary part of the dynamical variables.

For part of this study, we included complex Gaussian white noise terms $\eta_j(t) = \eta_{j,R}(t) + i\eta_{j,I}(t)$, where $j = 1, 2$, which satisfied $\langle \eta_{j,\alpha}(t)\eta_{k,\beta}(t')_t \rangle = \sigma^2\delta(t - t')\delta_{jk}\delta_{\alpha\beta}$, where $\langle \ldots_t \rangle$ denotes time average, j, $k = 1, 2$, and α, β denotes R or I. The noise variance, σ^2, was adjusted

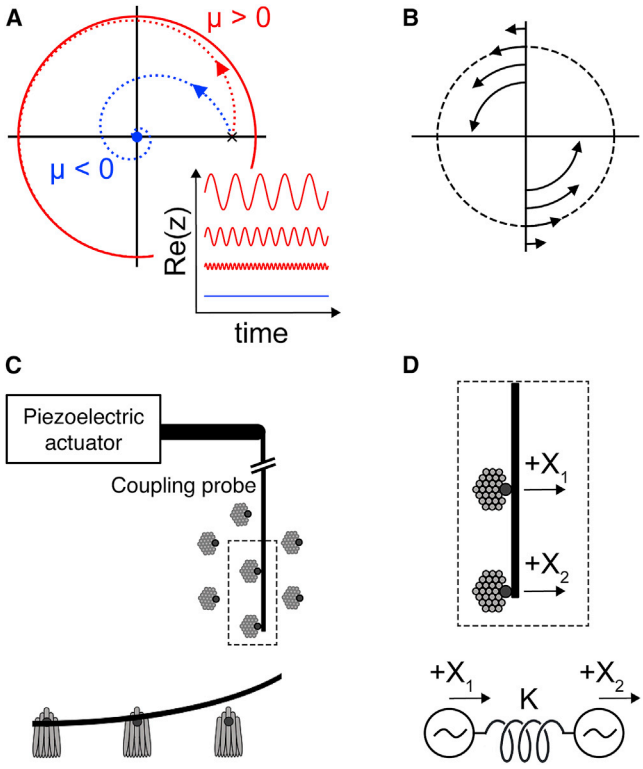

FIGURE 1 The complex displacement, $z(t)$, of a single, nonisochronous oscillator is described by $dz(t)/dt = (\mu + i\omega_0)z - (1 + i\beta)|z|^2 z$, when $\beta > 0$. (*A*) The complex phase plane is constructed by plotting the imaginary against the real component of $z(t)$. For $\mu > 0$, the trajectory originating from an arbitrary point in the phase plane converges to a limit cycle (*red line*). For $\mu < 0$, the trajectory (*blue dashed line*) terminates at a stable fixed point at the origin (*blue dot*). (*inset*) The oscillator's displacement is stationary for $\mu < 0$ (*blue line*) and oscillatory for $\mu > 0$ (*red lines*). From bottom to top, the oscillation amplitude increases with μ, whereas the frequency declines. (*B*) The complex phase plane illustrates the frequency-amplitude coupling of the nonisochronous oscillator for $\beta > 0$. Over a time interval, the trajectory at a higher value of μ traverses a shorter distance along the limit cycle than that with a smaller μ. This is associated with the decline in the angular velocity as the amplitude increases. (*C*) A schematic drawing depicts the glass fiber, with the tip of the coupling probe attached to two hair bundles in the planar epithelium of the bullfrog sacculus, observed from the top-down view of the epithelium. A side view diagram illustrates the curvature of the coupling probe that allows us to avoid contacting other nearby hair bundles. (*D*) The motion of each hair bundle is perpendicular to the coupling probe, with the positive direction pointing toward the kinociliary bulbs and the attachment point to the probe. The probe-bundles system is modeled as two autonomous oscillators coupled via an elastic element. To see this figure in color, go online.

such that the ratio between the root-mean-square displacement to the spectral amplitude approximately matched the experimental range. Numerical simulations of Eqs. 1 and 2 were performed using the fourth-order Runge Kutta method with a 10-ms time step. The initial conditions of both oscillators were chosen to be real and identical at $z_1(t = 0) = z_2(t = 0) = \mu^{1/2}$.

Biological preparation and measurement of hair-bundle displacement

All animal-handling protocols were approved by the University of California Los Angeles Chancellor's Animal Research Committee (Protocol Number ARC 2006-043-41A). Sacculi were excised from the inner ears of North American bullfrogs (*Lithobates catesbeianus*). The preparation was mounted into a two-compartment chamber in which the basal side was immersed in artificial perilymph (110 mM Na^+, 2 mM K^+, 1.5 mM Ca^{2+}, 113 mM Cl^-, 3 mM D-glucose, 1 mM sodium pyruvate, 1 mM creatine, and 5 mM HEPES) and the apical side in artificial endolymph (2 mM Na^+, 118 mM K^+, 0.25 mM Ca^{2+}, 118 mM Cl^-, 3 mM D-glucose, and 5 mM HEPES). The otolithic membrane was gently removed after 8-min enzymatic dissociation with 50 μg/ml collagenase IV (Sigma Aldrich, St. Louis, MO). For experiments in which calcium concentration of endolymph was varied, the preparation was initially immersed in low-calcium endolymph with 0.1 mM Ca^{2+}. The calcium level was increased by increments of 75 μM by adding 5 μL of $CaCl_2$ containing 100 mM Ca^{2+}.

Images of the preparation were recorded at 500 frames/s by a high-speed CMOS camera (Orca-Flash4.0; Hamamatsu, Shizuoka, Japan). The hair-bundle motion was tracked with a custom software written in MATLAB (The MathWorks, Natick, MA). The center position of the bundle was extracted by calculating the center of gravity of the intensity profile in each frame. A slow drift in the bundle displacement was removed by applying a second-order Savitzky-Golay filter to each 5-s segment of the recording.

Mechanical coupling of two hair bundles and stimulation

A borosilicate glass fiber was pulled with a micropipette puller (P97; Sutter Instruments, Novato, CA). An additional thin rod of ~100–200 μm, which served as a coupling probe, was fabricated at a 90° angle from the tip of the fiber using a microforge (Fig. 1 *C*). The curvature of the coupling probe was created out of the probe-fiber plane by placing its tip near the microforge. The difference in the temperatures of the two sides of the coupling probe resulted in a bending away from the heat source.

The fiber was placed with the coupling probe's tip parallel to the epithelium. To achieve a strong adhesion, the probe was attached to the kinociliary bulbs of both hair bundles. This configuration required that the bundles' axes of symmetry be nearly parallel to each other and perpendicular to the probe (Fig. 1 *C*; Supporting Materials and Methods, Section I). The motion of the coupling probe, driven by the bundles, was therefore in the transverse direction (Fig. 1 *D*). The probe's curvature allowed us to avoid other hair bundles on the preparation.

To calibrate the stiffness of the coupling probe, the motion of its tip in water was imaged at 10,000 frames/s, and its power spectral density was fitted by a Lorentzian function. The probes utilized in this work had stiffnesses of ~0.1–0.2 mN/m. To deliver sinusoidal stimulation at various frequencies, the base of the fiber was mounted on a piezoelectric stimulator (P-150; Piezosystem Jena, Hopedale, MA) and controlled with LabVIEW (National Instruments, Austin, TX). The probe base was driven along an axis parallel to the motion of the bundles by a discrete frequency sweep of sinusoidal signals at 30-nm amplitude. This corresponded to a maximal force of ~3–6 pN on a stationary hair bundle. The frequency was increased from 2.5 to 50 Hz at 2.5-Hz increments. Each stimulus frequency was presented for 20 cycles.

Data analysis

All analyses were performed in MATLAB. Time traces obtained from numerical simulations and hair-bundle displacement measurements from experiments were analyzed in a similar fashion. The oscillation amplitudes and frequencies were extracted by two methods. First, the spectral amplitude and spectral frequency were determined from the parameters of the Lorentzian fit to the amplitude spectrum. We calculated the finite-time Fourier transform on each nonoverlapping segment of the signal. The duration of each segment was 1 s for experimental recordings and 50 s for simulated traces. The amplitude spectrum was the averaged magnitude of the complex transform. For the second approach, we identified the local extrema of oscillations using a peak detection algorithm. All local extrema were determined from a

trace smoothed with a five-point moving average. The threshold for oscillation detection was defined to be 20% of the difference between the global maximum and minimum to exclude random fluctuations from the analysis. Any local maximum (minimum) whose displacement exceeded the adjacent minimum (maximum) by more than the threshold was identified as a peak (trough). The peak amplitude was computed by averaging half the difference between any adjacent peak and trough for the entire duration of the analyzed signal. Similarly, the peak-to-peak frequency was determined from the averaged reciprocal of the period between two neighboring peaks.

We quantified the degree of coherence of a spontaneous oscillation from the quality factor—the ratio between its peak spectral frequency and the full width at half maximum of the peak in the amplitude spectrum. In response to sinusoidal driving forces at various frequencies, the phase-locked amplitude was estimated from a sinusoidal fit to the average bundle displacement. A Lorentzian function was fitted to the plot of the response amplitude as a function of the driving frequency to extract the quality factor.

To compute the vector strength of the phase difference, the instantaneous phase of each time trace, denoted by $\phi_j(t)$, where $j = 1, 2$, was obtained from the Hilbert transform. The vector strength was defined as $V = \left|\left\langle e_t^{i\Delta\phi(t)}\right\rangle\right|$, where $\Delta\phi(t) = \phi_1(t) - \phi_2(t)$ denotes the oscillators' phase difference at time t. Perfectly phase-locked signals had a vector strength of unity, whereas uncorrelated signals had zero vector strength.

Hartigans' dip test statistic was used to indicate the crossing of a bifurcation of a noisy nonlinear system by quantifying the multimodality of position distributions. The algorithm measured the statistical difference between the empirical distribution and a uniform (null) distribution (29). A noisy motion underlaid by a limit-cycle oscillation possessed a large value of the dip test statistic, whereas random fluctuations around a stable fixed point corresponded to a small dip test statistic. The two behaviors were distinguished by the value of the dip test statistic with a threshold at 0.01 (13).

A two-dimensional phase space was reconstructed from experimental recordings to investigate the dynamical trajectory of the oscillator. The time trace was represented as the real part of an analytical signal whose imaginary part was obtained from the Hilbert transform of the oscillation (13). The distribution of the trajectory in the complex plane, termed the analytic distribution, was created from a two-dimensional histogram of the analytic signal. An analytic distribution with a loop structure corresponded to a limit-cycle oscillation, whereas a unimodal distribution corresponded to random fluctuations around a stable fixed point.

To estimate the critical control parameter μ_c of coupled oscillators from numerical simulations of the model, the initial positions of both oscillators were fixed at an identical, small value $\sim 10^{-4}$–10^{-3}. The oscillation amplitude decayed toward zero when poised in the stable regime, $\mu < \mu_c$, or grew toward a constant value corresponding to the radius of the limit cycle in the oscillatory regime, $\mu > \mu_c$. At the bifurcation, $\mu = \mu_c$, the duration of the transient solution diverged, and the oscillation profile remained relatively unchanged regardless of the initial condition. We extracted the time-dependent peak amplitude of the transient solution simulated at different values of μ and plotted its rate of change as a function of μ. The critical value, μ_c, was identified at the zero crossing. We increased the control parameter at 0.005 increments, which determined the resolution of the estimated μ_c. For the parameter space explored in this work, the critical values μ_c of both oscillators were identical within the 0.005 resolution.

RESULTS

Theoretical predictions

A system of two hair bundles connected to a glass probe was modeled as two mutually coupled nonlinear oscillators (Materials and Methods). The dynamics of the oscillators were described by the complex variables, $z_1(t)$ and $z_2(t)$, with their real parts representing the oscillators' displacements. $\omega_{0,1}$ and $\omega_{0,2}$ denote the characteristic frequencies, with $\omega_{0,2} \geq \omega_{0,1}$.

$$\frac{dz_1}{dt} = (\mu + i\omega_{0,1})z_1 - (1 + i\beta)|z_1|^2 z_1 + K(\mathrm{Re}(z_2) - \mathrm{Re}(z_1)) + \eta_1(t). \quad (1)$$

$$\frac{dz_2}{dt} = (\mu + i\omega_{0,2})z_2 - (1 + i\beta)|z_2|^2 z_2 + K(\mathrm{Re}(z_1) - \mathrm{Re}(z_2)) + \eta_2(t). \quad (2)$$

The coupling was mediated by an elastic element whose extension was the relative displacement of the oscillators, i.e., the difference in the real parts of $z_1(t)$ and $z_2(t)$. To describe the strong-coupling conditions experienced by the hair bundles connected by a short glass fiber, the coupling constant was set to be real and denoted by a stiffness K. Our model thus incorporated coupling only between the real components of the dynamical variables.

Critical control parameter of coupled oscillators

We first identified the critical control parameter μ_c of the coupled oscillators, at which the stability of the system transitioned between quiescent and oscillatory behavior. For $\mu > \mu_c$, the system displayed autonomous oscillations and remained at rest for $\mu < \mu_c$. In the absence of coupling, the critical point of a single oscillator was at $\mu_c = 0$ (Fig. 1 *A*). We estimated μ_c from the rate of change in the time-dependent peak amplitude of the transient oscillation (Materials and Methods). The rate became zero at criticality, $\mu = \mu_c$. Within the range of parameters explored in our study, μ_c of both oscillators remained nearly identical. Because the stability of the system near the critical point does not involve the nonlinear term, simulations were performed in the isochronous limit, $\beta = 0$, for simplicity.

When the oscillators' characteristic frequencies were nearly identical, $\omega_{0,1} \approx \omega_{0,2}$, μ_c remained close to zero and was unaffected by coupling (Fig. 2 *A*). With the introduction of a frequency difference, the critical point of the system shifted, with the magnitude of μ_c increasing over a range of low coupling constants, displaying a maximum, and declining toward zero at higher stiffnesses. The peak μ_c occurred at progressively larger coupling strengths as the characteristic frequencies diverged. The root-mean-square displacement, calculated from the steady-state solution of each oscillator, confirmed the existence of a quiescent regime for control parameters below μ_c (Fig. 2 *B*).

When the control parameters were fixed at a sufficiently large value, the self-sustained motion displayed higher-order mode locking at low coupling coefficients (Fig. 2 *C*). A slight increase in the stiffness of the coupling element suppressed the oscillations, as μ_c exceeded the control parameter of each oscillator. Synchronized limit-cycle oscillations then emerged again at high coupling constants with unity vector

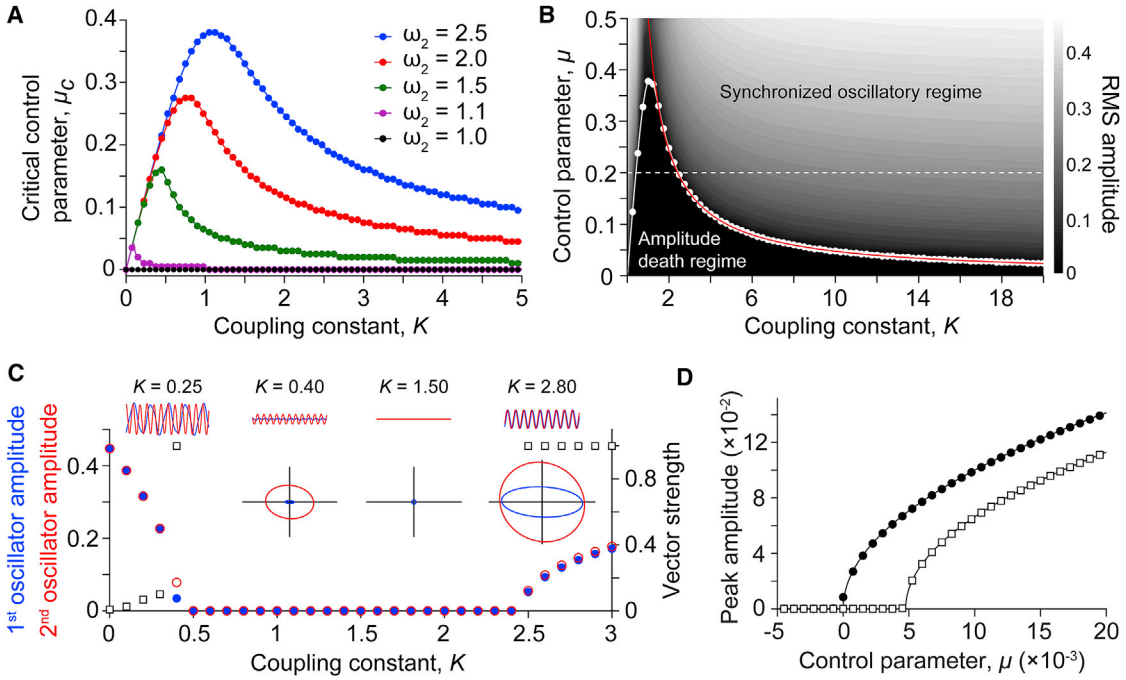

FIGURE 2 The critical control parameter (μ_c) of coupled oscillators. In all panels, $\omega_{0,1}$ is fixed at 1. (*A*) μ_c is estimated from the rate of amplitude change of the transient solution obtained from numerical simulations. The estimated μ_c remains at zero for identical oscillators: $\omega_{0,1} = \omega_{0,2} = 1$ (*black dots*) and progressively increases upon growth of the difference between the characteristic frequencies: $\omega_{0,2} = 1.1$ (*magenta*), $\omega_{0,2} = 1.5$ (*green*), $\omega_{0,2} = 2.0$ (*red*), and $\omega_{0,2} = 2.5$ (*blue*). μ_c-values calculated from a linear stability analysis of the model are consistent with the estimated values (*solid lines*). (*B*) A state diagram of coupled oscillators with $\omega_{0,2} = 2.5$ incorporates the line of supercritical Hopf bifurcation whose μ_c is estimated from numerical simulations (*white dots*) and calculated from Eq. 3 (*white solid line*). The heat map illustrates theroot-mean-square amplitude of the first oscillator, with brighter shades representing higher values. The oscillators are arrested when $\mu < \mu_c$ ("amplitude death"). The vector strength of the oscillators' phase difference reaches unity over a regime with sufficiently large coupling constant or control parameter ("synchronized oscillation"). The onset of the regime is indicated by a red solid line interpolated from the smallest K that results in the unity vector strength obtained from numerical simulations. (*C*) uses the same parameters as in (*B*) with μ fixed at 0.2 (*white dashed line* in *B*). The amplitudes of the first (*blue dots*) and second (*red open dots*) oscillators vanish when $K \sim 0.5$–2.4. The vector strength of the phase difference (*squares*) indicates the absence of one-to-one phase locking for weak coupling and the onset of synchronization for $K > 2.4$. The time traces of both oscillations at different coupling constants illustrate the suppression of oscillatory activity (*upper insets*, *blue lines*: first oscillator, *red lines*: second oscillator). The phase portraits at the corresponding coupling constant reveal a stable fixed point at the origin of the complex plane, an indication of an amplitude death regime (*lower insets*). (*D*) At $K = 100$, the peak amplitude of the synchronized oscillation increases with the control parameter. μ_c is zero for a small frequency difference ($\omega_{0,2} = 1.1$, *black dots*) and is positive for a large frequency difference ($\omega_{0,2} = 2.5$, *squares*). Solid lines illustrate results from the fit: $\mu^{1/2}$ for $\omega_{0,2} = 1.1$ and $0.915(\mu - 4.75 \times 10^{-3})^{1/2}$ for $\omega_{0,2} = 2.5$.

strength of their phase difference (Fig. 2, *B* and *C*). These results indicated that, with a large frequency difference, oscillators individually poised in the oscillatory regime may be brought near a critical point or into the quiescent regime by adjusting the strength of coupling. Further, the small value of μ_c at high stiffnesses suggested that strongly coupled oscillators could display synchronized autonomous oscillations despite a large difference in their characteristic frequencies.

We illustrated the dynamics of coupled oscillators in the complex phase space, constructed from the real and imaginary part of $z_1(t)$ and $z_2(t)$. For isolated oscillators with $\mu > 0$, the phase-space trajectories followed limit cycles, centered around an unstable fixed point at the origin (Fig. 1 *A*). In the presence of coupling with an appropriate strength, the fixed point became stable, and both phase-space trajectories were consequently attracted to the origin, resulting in the suppression of autonomous motion (Fig. 2 *C*). This indicated an "amplitude death" regime in association with the shift in μ_c (30,31). Upon an increase in the coupling constant, the fixed point lost its stability, and limit cycles emerged. Note that although the oscillators displayed synchronized motion, the two limit cycles were nonidentical. This was due to the different imaginary components of their dynamical variables, as the coupling only affected the real parts.

A linear stability analysis of Eqs. 1 and 2 showed that for nearly identical oscillators, $\omega_{0,2}/\omega_{0,1} \simeq 1$, a supercritical Hopf bifurcation occurred at $\mu_c \sim (\omega_{0,2} - \omega_{0,1})^2/4K$ (Supporting Materials and Methods, Section II). On the other hand, at a sufficiently large frequency difference, $\omega_{0,2}/\omega_{0,1} \gtrsim 2$, μ_c satisfied

$$\omega_{0,1}^2\omega_{0,2}^2 + \left(\omega_{0,1}^2 + \omega_{0,2}^2\right)\left(\mu_c^2 - K\mu_c\right) - 2K\mu_c^3 + \mu_c^4 = 0. \tag{3}$$

Numerical solutions of μ_c as a function of K from Eq. 3 agreed with results from simulations, verifying consistency

between the simulations and analytic estimates (Figs. 2, *A* and *B* and S1).

To facilitate comparisons to the experimental data, we focused on the strong-coupling limit, in which the stiffness was fixed at a large value (Supporting Materials and Methods, Section 1); the coupling coefficient was kept constant at $K = 100$ for the rest of our study. The oscillation amplitude obtained from numerical simulations of the model was proportional to $(\mu - \mu_c)^{1/2}$, characteristic of a system near a supercritical Hopf bifurcation (Fig. 2 *D*). We note that in this strong-coupling limit, nearly identical oscillators with appropriate initial positions could display an oscillation death behavior when $\mu > \mu_c$ (Supporting Materials and Methods, Section III).

Dynamics of synchronized oscillations far from a bifurcation

Next, we investigated the behavior of synchronized limit-cycle oscillations far from criticality, $\mu > \mu_c$. We focused on this regime because free-standing hair bundles from the bullfrog sacculus typically display robust large-amplitude spontaneous oscillations under in vitro conditions and thus seem to be innately poised far from the quiescent regime. Because of the nonisochronous characteristics displayed by the spontaneous motion of individual hair bundles, we explored the effects of the degree of nonisochronicity on the dynamics of synchronized oscillators.

In the oscillatory regime, far from the bifurcation, the oscillators displayed two classes of behavior, dependent on their degrees of nonisochronicity β. For small β, synchronized oscillations displayed similar features to those of isochronous (Fig. 2 *D*) or uncoupled oscillators (Fig. S3). The peak amplitude of the oscillation rose monotonically as the control parameter was increased (Fig. 3 *A*). Because of the positive β, the peak-to-peak oscillation frequency declined upon growth of the amplitude.

When β was sufficiently large, the limit-cycle amplitude displayed a broad peak with the maximum occurring between control parameter values 0.5 and 1.0 (Fig. 3, *D* and *G*). For oscillators with a small frequency difference, the tuning was due to the suppression of oscillations within a narrow range of control parameter values between 0.9 and 1.1 (Fig. 3 *D*). On the other hand, oscillators with a large frequency difference exhibited the maximal amplitude that approximately coincided with the minimum in the oscillation frequency (Fig. 3 *G*).

Next, we elucidated the mechanism underlying the peak oscillation amplitude by illustrating the complex phase plane constructed from the real and imaginary parts of $z_1(t)$ and $z_2(t)$. We found that the tuning behavior was associated with the original oscillation frequency of individual oscillators displayed in the absence of coupling. In polar coordinates, the angular equation for the j^{th} oscillator, in the absence of coupling, was given by $\Omega_j = d\phi_j(t)/dt = \omega_{0,j} - \beta R_j^2$, where $z_j(t) = R_j e^{i\phi_j(t)}$, and $j = 1$ or 2. For $\beta > 0$, the frequency of each oscillator declined upon an increase in μ. In turn, the angular velocity diminished and went to zero when the radius satisfied $R_j^2 = \mu_{0,j} = \omega_{0,j}/\beta$. Therefore, at $\mu = \mu_{0,1}$ or $\mu_{0,2}$, the trajectory of one of the oscillators terminated at a point on a circle in the phase space, termed an angular nullcline.

In contrast to nearly identical coupled oscillators, which exhibited similar trajectories in the phase portraits (Figs. 3 *D* and S2), coupled oscillators with a large frequency difference displayed stable limit cycles with drastically distinct shapes (Fig. 3, *A* and *G*). Because the imaginary component of $z_1(t)$ oscillated about a nonzero offset, the first oscillator's trajectory was approximately elliptical and situated on the upper perimeter of the second oscillator's limit cycle. With different initial positions of the oscillators, this offset might become negative. This behavior thus exhibited a bistability in which the first trajectory could instead be confined to the lower half of the complex plane. For small β, the range of control parameters investigated did not approach the angular nullclines as $\mu << \omega_{0,j}/\beta$, thus resulting in the monotonically varying limit-cycle amplitudes and frequencies of both oscillators (Fig. 3 *A*). For large β and small frequency difference, the limit-cycle trajectories terminated at two distinct points in the vicinity of the angular nullclines when $\mu \approx \mu_{0,1}$ and $\mu_{0,2}$ (Fig. 3 *D*), indicative of an oscillation death regime (Supporting Materials and Methods, Section III). This quiescent behavior gave rise to a local maximum in the limit-cycle amplitude within a range $\mu_c < \mu < \mu_{0,1} \approx \mu_{0,2}$. The system displayed stable, synchronized limit cycles at higher values of the control parameter. In contrast, oscillators with a large frequency difference reached the peak in their oscillation amplitude and a minimal frequency when the trajectory of the first oscillator approached its angular nullcline, $\mu \approx \mu_{0,1}$. A larger control parameter led to the separation of the two limit cycles as well as an attenuation of the oscillation amplitude (Fig. 3 *G*).

Finally, we introduced Gaussian white noise into Eqs. 1 and 2 to account for the noisy nature of hair bundles' motion. The features of noisy oscillations were extracted from the amplitude spectra obtained from a finite-time Fourier transform. As in the deterministic case, the dynamics of the oscillators possessed two classes of behaviors far from the critical point (Fig. 3, *B*, *E*, and *H*).

We quantified the coherence of the oscillations by the ratio of the spectral frequency to the full width at half the maximum of the peak in the amplitude spectrum (Materials and Methods). Near criticality, the degree of coherence was enhanced as the oscillators crossed the bifurcation point and entered the oscillatory regime. As the control parameter continued to increase, the degree of coherence reached a plateau for weakly nonisochronous oscillators (Fig. 3 *C*), whereas a nonmonotonic behavior was observed in oscillators with a large β. For nearly identical oscillators, the vanishing oscillation frequency or amplitude led to a minimal degree of coherence over a broad range of the control

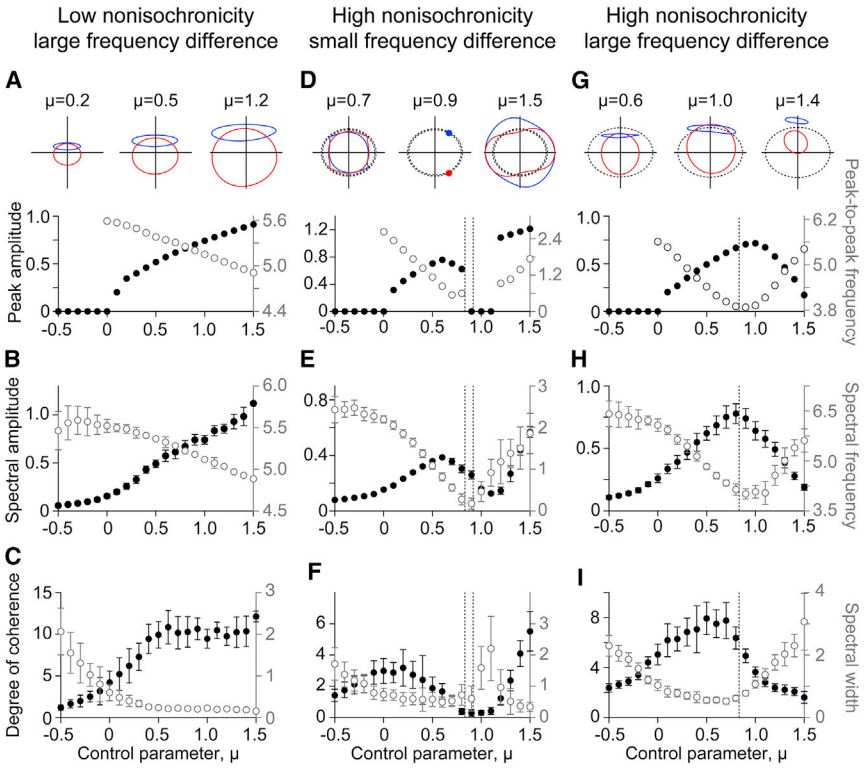

FIGURE 3 Dynamics of coupled oscillators far from criticality. The parameters are $\omega_{0,1} = 2.5$ and $K = 100$. In panels in which noise is included, the noise variance is $\sigma^2 = 4$, and error bars indicate standard deviation (SD) of data obtained from 10 simulations. In (*A*)–(*C*), $\beta = 0.5$ and $\omega_{0,2} = 7.5$. (*A*) In the absence of noise, weakly nonisochronous oscillators display a monotonic increase in the peak amplitude of the oscillation (*black dots*) and a decline in the peak-to-peak frequency (*open gray dots*) upon growth of the control parameter in the oscillatory regime. (*Inset*) The phase portraits at the corresponding control parameter reveal the distinct shapes of the limit cycles (*blue lines*: first oscillator, *red lines*: second oscillator). (*B*) When Gaussian white noise is included, the spectral amplitude (*black dots*) and spectral frequency (*open gray dots*) exhibit qualitatively identical behaviors as in the deterministic limit. (*C*) The degree of coherence of the autonomous motion is enhanced (*black dots*) as the width of the spectral peak decreases (*open gray dots*) when the system enters the oscillatory regime. In (*D*)–(*F*), $\beta = 3$ and $\omega_{0,2} = 2.75$. The vertical dashed lines indicate the control parameters at the angular nullclines of the first and second oscillators ($\mu_{0,1} = 0.83$ and $\mu_{0,2} = 0.92$). (*D*) Far from criticality, strongly nonisochronous oscillators with a small frequency difference are arrested in the absence of noise. (*Inset*) The phase portraits illustrate the stable fixed points in the vicinity of the angular nullclines (*dashed lines*). (*E*) With random fluctuations, the system exhibits tuned behavior. (*F*) The coherence becomes minimal over a range of the control parameter coinciding with diminishing amplitude. In conjunction with this, the spectral peak reaches a maximum. In (*G*)–(*I*), $\beta = 3$ and $\omega_{0,2} = 7.5$. The vertical dashed line indicates the control parameter at the angular nullcline of the first oscillator ($\mu_{0,1} = 0.83$). (*G*) In the deterministic limit, strongly nonisochronous oscillators with a large frequency difference show a peak in the spectral amplitude and a minimum in the frequency near the angular nullcline. (*Inset*) The limit cycles separate in association with the reduction of the oscillation amplitude, as the control parameter exceeds the value at the angular nullcline. (*H*) Qualitatively similar behaviors are observed upon addition of noise. (*I*) The degree of coherence exhibits a peak near the maximal spectral amplitude. Within the same range of the control parameter, the width of the spectral peak reaches a minimum.

parameter (Fig. 3 *F*). Hence, a peak coherence was observed close to the critical point. In contrast, the motion of oscillators with a large frequency difference became more regular as the oscillation amplitude increased. Therefore, the degree of coherence, as well as the amplitude, reached their maxima over the same range of control parameters (Fig. 3 *I*).

Experimental observations

We attached the tip of a thin, bent glass probe to two neighboring oscillatory bundles in the planar epithelium of the bullfrog sacculus and observed their dynamics under high coupling stiffness (Supporting Materials and Methods, Section I). The curvature of the tip of the probe enabled us to avoid other hair bundles on the preparation (Fig. 1 *C*).

Synchronized spontaneous oscillations of coupled hair bundles

When immersed in an artificial endolymph with 250 μM calcium, the concentration near the physiological level, coupled hair bundles oscillated spontaneously with a pronounced peak in the amplitude spectrum (Fig. 4, *A* and *B*). The bundles always moved in synchrony with the vector strength of their phase difference exceeding 0.9. These synchronized spontaneous oscillations were observed despite the large difference in their natural frequencies measured in the absence of an attached fiber. We occasionally found that the motion of some coupled hair bundles resembled rapid fluctuations, with the amplitude spectra displaying a weak but distinct broad peak at high frequency.

We studied the effects of coupling on the fluctuation levels by extracting the degree of coherence of coupled and uncoupled hair bundles. Because the effects of thermal noise depended greatly on the geometry and stiffness of the system, we compared the regularity of coupled hair bundles' oscillations to those of single bundles, each attached to a probe with comparable stiffness and drag coefficients. Because hair bundles could sustain microscopic damage upon removal of the fiber, thus affecting their dynamics, these comparisons were performed on data sets obtained from two distinct groups of hair cells. We found that the average degrees of coherence in both cases were comparable (Fig. 4 *C*): 1.11 ± 0.82 (n = 15) for single bundles and 1.09 ± 0.69 (n = 26) for coupled bundles. In addition, the degree of coherence was not significantly different from free-standing bundles with no fiber attached: 1.11 ± 0.94 (n = 20).

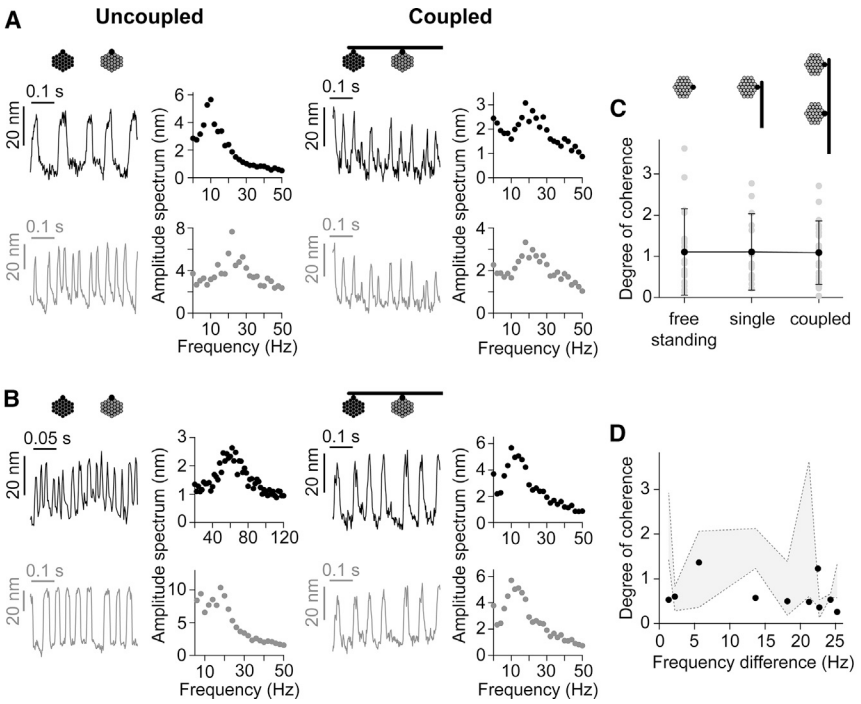

FIGURE 4 Synchronized spontaneous oscillations of hair bundles. (*A* and *B*) (*Left panels*, "Uncoupled") Two examples of spontaneous oscillations of two pairs of hair bundles in the absence of coupling. (*Right panels*, "Coupled") Upon coupling, the displacements of the two bundles become nearly identical. The corresponding amplitude spectra are shown to the right of the time traces. Error bars are the SDs from the finite-time Fourier transform. (*C*) The average degree of coherence (*black dots*) of hair bundles under three types of mechanical manipulations is shown: unloaded ("free standing"), loaded without coupling to another bundle ("single"), and coupled bundles ("coupled") are 1.11 ± 0.94 (n = 20), 1.11 ± 0.82 (n = 15), and 1.09 ± 0.69 (n = 26), respectively. Error bars indicate SD of the data from individual hair bundles (*gray dots*). (*D*) The degree of coherence of synchronized oscillations (*black dots*) is independent of the bundles' characteristic frequencies or their regularity in the absence of coupling. The degree of coherence of the two uncoupled hair bundles is illustrated by the upper and the lower bounds of the gray area.

We recorded the motion of pairs of free-standing hair bundles before the coupling and extracted their degree of coherence. We found that in contrast to previous predictions (21,25), neither a small frequency difference nor a high regularity of the uncoupled oscillations improved the coherence of the synchronized motion (Fig. 4 *D*). This contradiction could partly stem from the variations in the degree of nonisochronicity of the bundles. Our theoretical predictions suggested that the coherence of synchronized oscillations that were far from the bifurcation depended on the frequency difference and the coefficient β in a complex manner (Fig. 3, *C*, *F*, and *I*).

Coupled hair-bundle motility near the critical point

Next, we employed the variation of calcium concentration in the endolymph as an experimental modulation of the control parameter. The level of calcium was increased from 100 μM in 75-μM increments (Materials and Methods). In this section, we focus on the dynamics of hair bundles at high calcium concentrations, near the critical level (Fig. 5, *shaded areas*). The behavior of spontaneous oscillations at lower calcium levels will be discussed in the next section.

We utilized two metrics previously developed to study the behavior of noisy hair-bundle motility near the transition between the oscillatory and quiescent regimes (Materials and Methods) (13). Hartigans' dip test statistic was used to identify the crossing of a bifurcation by measuring the degree of multimodality in the distribution of a bundle's position. We further characterized the dynamics of hair-bundle oscillations by reconstructing an analytical signal whose two-dimensional histogram could reveal an underlying stable limit cycle or a stable fixed point in the complex phase space. We note that this reconstructed phase space differed from the previously discussed complex phase plane (Figs. 2 and 3) because the experimental time traces contained only the real components of the complex variables.

The critical range of calcium concentration was indicated by the Hartigans' dip test statistic crossing the threshold of multimodality (Fig. 5, *E* and *K*). This signified crossing of a bifurcation; an increase in the calcium level corresponded to a decrease in the control parameter from an oscillatory regime toward a quiescent regime. As the concentration approached a critical range, typically exceeding ~300 μM, hair-bundle motion could become highly asymmetric, with the oscillations spending more time in the positive or negative displacement (Fig. 5, *A* and *G*). Because of the nonsinusoidal oscillation profile, we extracted the oscillation amplitude and frequency from both the amplitude spectrum and local extrema in the time trace. As the calcium level increased, the spectral and peak amplitudes of synchronized spontaneous oscillations were attenuated, until they became indistinguishable from random fluctuations (Fig. 5, *B* and *H*). In association with this, the peak-to-peak frequency increased and became undefined as the oscillations were suppressed (Fig. 5, *C* and *I*). The spectral frequency, on the other hand, remained relatively constant as the spectral peak was predominantly broadened, rendering the determination of the peak frequency less reliable.

The analytic distribution in a two-dimensional phase space formed a ring-like structure at low calcium concentrations.

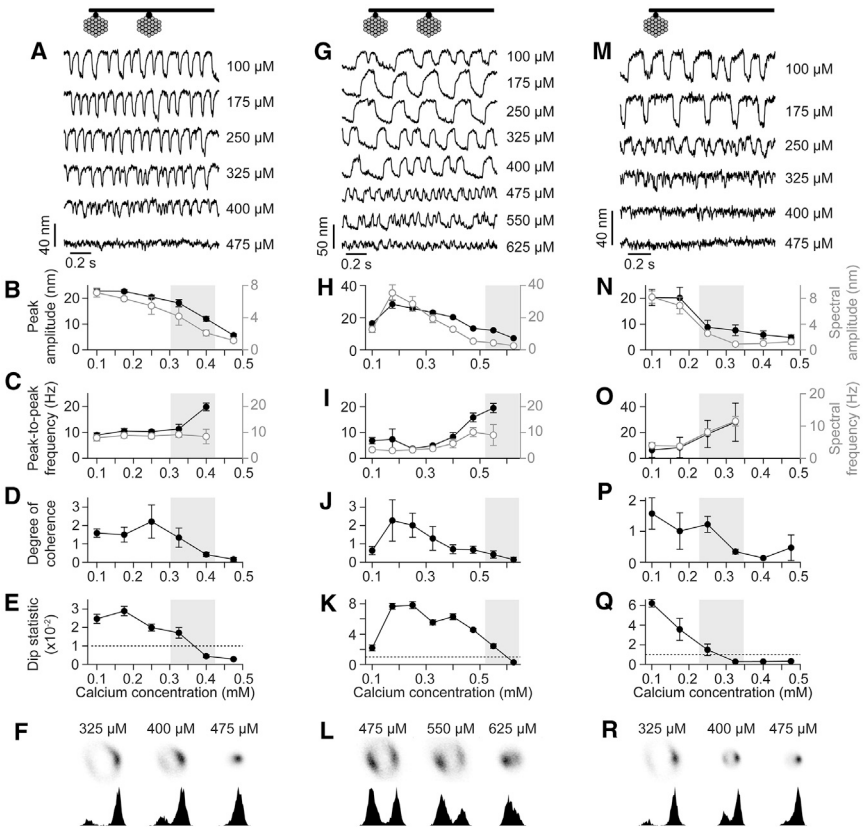

FIGURE 5 Synchronized spontaneous oscillations under calcium manipulation. (*A*) Coupled hair bundles' oscillations at different calcium levels are shown, indicated to the right of each trace. In (*B*)–(*E*), shaded areas indicate the transition regime from oscillatory to quiescent behavior. (*B*) The peak and spectral amplitude monotonically decrease as calcium level is elevated. (*C*) The peak-to-peak and spectral frequency remain relatively unchanged. In the transition regime, the peak-to-peak frequency increases, whereas the spectral frequency is poorly determined. At a higher calcium level, the hair-bundle motion becomes indistinguishable from a random fluctuation, and the oscillation frequency cannot be extracted. (*D*) The degree of coherence of spontaneous oscillations is minimally affected at lower calcium levels and gradually declines in the transition regime. (*E*) The Hartigans' dip test statistic, in association with the oscillation amplitude, decreases with increasing calcium levels. (*F*) The analytic distribution (*top panels*), as well as the displacement histogram (*bottom panels*), shows a transition from a ring-like structure to a unimodal distribution. In the transition regime, the oscillation spends longer fractions of time deflected in the positive direction. (*G*) Another type of behavior is observed from coupled hair bundles, whose oscillations become larger at 175–250 μM calcium. The calcium levels are indicated to the right of each trace. (*H–L*) A peak in the oscillation amplitude, degree of coherence, and the dip test statistic is observed near the physiological calcium level. (*M*) An example of a single bundle's displacement loaded by a glass fiber is given at various calcium levels indicated to the right of each trace. (*N–R*) The oscillation behaviors qualitatively resemble the first type of coupled hair bundles (*A–F*). In all cases, coupled or uncoupled hair bundles display similar behaviors in the transition regime (*shaded areas*). Error bars indicate the SD of the data extracted from six time trace segments; each is 10 s.

The ring decreased in size and converged to a unimodal distribution upon increasing the calcium concentration (Fig. 5, *F* and *L*). We note that at the levels of calcium concentration employed in this study, we did not observe an analytical distribution that corresponded to a coexistence of a limit cycle and a stable fixed point at the origin. Our results predominantly indicated that the behavior of coupled hair bundles across the critical calcium concentration was consistent with a supercritical Hopf bifurcation. Qualitatively identical dynamics were observed in single hair bundles under similar mechanical loading (Fig. 5, *M–R*).

Tuning behavior of synchronized spontaneous oscillations

In this section, we investigated the dynamics of hair bundles at lower calcium levels, far from criticality, and compared them with the theoretical predictions of coupled oscillators far from a supercritical Hopf bifurcation (Fig. 3).

In agreement with results from the model, we found two types of behaviors of synchronized spontaneous oscillations at low calcium levels. First, some coupled hair bundles showed a monotonic decrease in their oscillation amplitude and the degree of coherence as the calcium was elevated, predominantly consistent with a system of coupled, weakly nonisochronous oscillators (Fig. 5, *B–D*). The oscillation frequency, however, could remain largely unaffected (Fig. 5 *C*) or continually increase (Figs. 5 *I* and S4). On the other hand, the motion of some hair bundles displayed maximal amplitude and coherence at an optimal calcium concentration, typically near the physiological level of 250 μM (Figs. 5, *H–J* and S4). Within the same range of calcium concentrations, the peak-to-peak frequency of the oscillation clearly exhibited a minimum. This type of behavior agreed with a system of oscillators with a high degree of nonisochronicity.

To examine the frequency selectivity of coupled hair bundles at different calcium levels, we measured the bundles' displacements in response to pure-tone stimulation. Sinusoidal signals at various frequencies were delivered to the base of the glass fiber at a constant amplitude (Materials and Methods). The quality factor of the phase-locked amplitude displayed a similar calcium dependence as that shown by the degree of coherence of spontaneous oscillations (Fig. S5).

DISCUSSION

We observed synchronization between the autonomous motion of two strongly coupled hair bundles from the bullfrog

sacculus. Our experimental findings were well reproduced by a theoretical model of coupled nonlinear oscillators, each displaying a supercritical Hopf bifurcation. Results from the model indicated that strong coupling minimally affected the dynamical states of the oscillators. This suggested that the oscillatory hair bundles, despite their vastly different natural frequencies, remained unstable upon coupling, yielding the observed synchronized spontaneous oscillations. The theoretical prediction also implied that the existing mathematical descriptions of uncoupled hair bundles should be applicable to a small number of bundles under strong coupling.

Under weaker coupling, on the other hand, the model demonstrates that unstable oscillators with different characteristic frequencies may be brought closer to a supercritical Hopf bifurcation by a shift in the critical point. Hence, although the control parameter of each individual oscillator is unaffected, the coupling shifts the bifurcation point closer to them. The result implies that spontaneously oscillating hair bundles may become quiescent upon mechanical coupling of appropriate strength. Under physiological conditions, groups of hair bundles in the inner ears of many species experience weak coupling at large spatial separations. Our theoretical prediction thus proposes an additional potential mechanism of tuning a system of oscillatory hair bundles closer to criticality via mechanical coupling. Other physical quantities have been proposed to poise an uncoupled hair bundle near the verge of an instability; examples include mass, elastic loadings, and a stationary offset on the bundle's resting position imposed by its surrounding structure (12,15,32). A combination of these may be utilized as a mechanism that effectively brings an in vivo system of hair bundles near the critical point.

Although strong mechanical coupling did not affect the control parameters determining the dynamical states of individual hair bundles, it could qualitatively alter the dynamics of the coupled system in the oscillatory regime far from the critical point. We modulated the dynamical state of coupled hair bundles using the level of calcium concentration in the endolymph. We found that the amplitude, as well as the degree of coherence, of coupled hair bundles' autonomous oscillations could be enhanced near the physiological calcium concentration. This was associated with the peak in the quality factor of hair bundles' motion in response to sinusoidal stimuli. Our theoretical predictions revealed that this tuning behavior required an optimal degree of hair-bundle nonisochronicity.

Several studies have demonstrated the nonisochronous behavior of uncoupled hair bundles. The frequency of spontaneous oscillations was shown to decline upon growth in amplitude under different types of manipulations, including a change in calcium concentration, loading by a mass or an elastic element, and an application of a constant force (15,33). A high degree of nonisochronicity has been demonstrated to be beneficial to the detection of rapidly varying signals by poising the bundles in a chaotic regime in the presence of noise and thus enhancing the temporal resolution (34). Additionally, a lowered detection threshold was observed at an optimal level of nonisochronicity.

Our experimental observations also illustrated the nonisochronous characteristics of strongly coupled hair bundles upon changing the level of calcium concentration in the endolymph. As the calcium level was raised, the oscillation frequency increased in association with an attenuation in the amplitude. Our findings thus suggest the role of mechanical coupling on the spontaneous dynamics, as well as signal detection, of nonisochronous hair bundles. At an optimal degree of hair-bundle nonisochronicity, the system achieves its maximal frequency selectivity near the physiological calcium concentration. This proposes the control of the degree of nonisochronicity as an additional mechanism that shapes the frequency selectivity of a small number of hair bundles under strong mechanical coupling.

Possible mechanism underlying hair-bundle nonisochronicity

Spontaneous oscillations of hair bundles arise from the gating of the mechanosensitive ion channels, whose open probability is regulated by the tension in a tip link, a thin filament that serves as a component of the gating spring. Several microscopic models of hair-bundle mechanics have shown that the oscillation amplitude and frequency crucially depend on the stiffness of the gating spring, which dictates the nonlinearity of the system (11,12,35). Further, alterations in the spontaneous oscillation profiles under various forms of mechanical or chemical manipulation are well reproduced by models in which the gating-spring stiffness is reduced upon an increase in external calcium (33).

To test whether the calcium-sensitive gating-spring stiffness may contribute to hair-bundle nonisochronicity, we performed numerical simulations of the model previously shown to describe individual hair-bundle motility (33) and observed the spontaneous oscillations at different levels of calcium sensitivity. The model postulated that the gating spring incorporated a calcium-binding site whose binding probability p_{gs} depended on the local calcium concentration $[Ca^{2+}]_{gs}$ and followed the standard rate equation $dp_{gs}/dt = k_{gs,on}[Ca^{2+}]_{gs}(1 - p_{gs}) - k_{gs,off}p_{gs}$. The rates of binding and unbinding of calcium to the gating spring are denoted by $k_{gs,on}$ and $k_{gs,off}$, respectively. The gating-spring stiffness K_{gs} was governed by $K_{gs} = K_{gs,0} - K_{gs,1}p_{gs}$, in which $K_{gs,0}$ and $K_{gs,1}$ are positive constants.

We found that the spontaneous oscillations exhibited by a hair bundle with a constant gating-spring stiffness, $K_{gs,1} = 0$, were minimally dependent on the calcium concentration (Fig. 6 *A*). The autonomous motion abruptly diminished at a critical calcium level. When the gating-spring stiffness was modulated by calcium, the oscillation amplitude was attenuated, and the frequency increased upon a rise in the

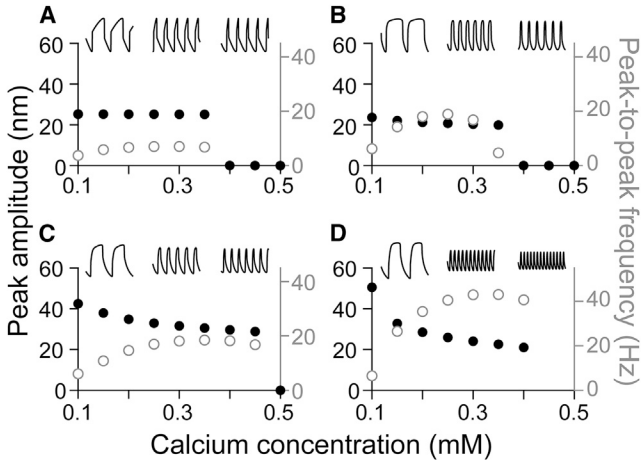

FIGURE 6 Nonisochronicity of a single hair bundle with a calcium-sensitive gating-spring stiffness. Results are obtained from numerical simulations of a model of hair-bundle motility. The parameter values are shown in Table S1. In all panels, the peak amplitude (*black dots*) and the peak-to-peak frequency (*open gray dots*) of hair-bundle spontaneous oscillations at different calcium concentrations are shown. The insets illustrate the time traces of spontaneous oscillations at calcium concentrations 0.1, 0.2, and 0.3 mM (from *left* to *right*). (*A*) When the gating-spring stiffness is a constant, with $K_{gs,0} = 1050$ μN/m and $K_{gs,1} = 0$, the oscillation profiles are not sensitive to calcium. (*B*) For a small calcium sensitivity, with $K_{gs,0} = 1300$ μN/m and $K_{gs,1} = 500$ μN/m ($K_{gs,1}/K_{gs,0} = 0.38$), the oscillation frequency increases with calcium level, whereas the amplitude is slightly attenuated. (*C*) The decline in the oscillation amplitude becomes more pronounced at a higher calcium sensitivity of the gating spring, with $K_{gs,0} = 2000$ μN/m and $K_{gs,1} = 1200$ μN/m ($K_{gs,1}/K_{gs,0} = 0.6$). (*D*) At $K_{gs,0} = 2550$ μN/m and $K_{gs,1} = 2000$ μN/m ($K_{gs,1}/K_{gs,0} = 0.78$), the nonisochronous behavior is strong, with the oscillation frequency rapidly increasing upon an attenuation in amplitude.

calcium level, a feature that is consistent with a nonisochronous nonlinear oscillator. At a higher calcium sensitivity ($K_{gs,1}/K_{gs,0}$), the hair bundle displayed a stronger nonisochronous behavior; its oscillation frequency more steeply depended on the amplitude as the calcium concentration increased (Fig. 6, *B–D*). These results suggest that a calcium-sensitive elastic element may partly account for the hair bundle's nonisochronicity.

CONCLUSION

We investigate the influence of mechanical coupling on the innate motility of hair bundles poised in different dynamical states. Results from a model of two nonisochronous oscillators, whose real parts of the complex dynamical variables are mutually coupled, suggest an alternative mechanism that tunes a system of weakly coupled unstable oscillators closer to criticality via a shift of the bifurcation point. Theoretical predictions for strongly coupled oscillators are consistent with the dynamics of hair bundles under strong mechanical coupling. Within a critical range of calcium concentration in the endolymph, synchronized spontaneous oscillations of hair bundles become suppressed and exhibit characteristics of a nonlinear system crossing a supercritical Hopf bifurcation, identical to single hair bundles. At calcium levels sufficiently far from the critical point, hair bundles may display a tuning in the amplitude and coherence of their spontaneous oscillations, as well as a tuning of the quality factor in response to an external driving force. This behavior was observed in the model with highly nonisochronous oscillators, suggesting that hair bundles' nonisochronicity might play a role in optimizing the frequency selectivity of the coupled system near the physiological calcium level. Further, results from a microscopic model of a single hair bundle's motility indicate that nonisochronicity may stem from a calcium-sensitive elastic element that controls the gating of the mechanosensitive ion channels.

SUPPORTING MATERIAL

Supporting Material can be found online at https://doi.org/10.1016/j.bpj.2020.11.2273.

AUTHOR CONTRIBUTIONS

Y.R. designed the research, conducted physiological recordings and theoretical analysis, and wrote the manuscript. J.F. designed the research, performed theoretical analysis, and wrote the manuscript. D.B. supervised the research and wrote the manuscript.

ACKNOWLEDGMENTS

D.B. gratefully acknowledges support of the National Science Foundation Biomechanics and Mechanobiology Program, under grant 1916136. Y.R. acknowledges support by Chulalongkorn University: CU_GR_62_71_23_28, and Chulalongkorn University Office of International Affairs Scholarship for Short-term Research (3/2562).

SUPPORTING CITATIONS

References (36–38) appear in the Supporting Material.

REFERENCES

1. Hudspeth, A. J. 2014. Integrating the active process of hair cells with cochlear function. *Nat. Rev. Neurosci.* 15:600–614.
2. Robles, L., and M. A. Ruggero. 2001. Mechanics of the mammalian cochlea. *Physiol. Rev.* 81:1305–1352.
3. Martin, P., A. D. Mehta, and A. J. Hudspeth. 2000. Negative hair-bundle stiffness betrays a mechanism for mechanical amplification by the hair cell. *Proc. Natl. Acad. Sci. USA.* 97:12026–12031.
4. Kennedy, H. J., A. C. Crawford, and R. Fettiplace. 2005. Force generation by mammalian hair bundles supports a role in cochlear amplification. *Nature.* 433:880–883.
5. Jaramillo, F., and A. J. Hudspeth. 1993. Displacement-clamp measurement of the forces exerted by gating springs in the hair bundle. *Proc. Natl. Acad. Sci. USA.* 90:1330–1334.
6. Martin, P., and A. J. Hudspeth. 1999. Active hair-bundle movements can amplify a hair cell's response to oscillatory mechanical stimuli. *Proc. Natl. Acad. Sci. USA.* 96:14306–14311.

7. Ricci, A. J., A. C. Crawford, and R. Fettiplace. 2000. Active hair bundle motion linked to fast transducer adaptation in auditory hair cells. *J. Neurosci.* 20:7131–7142.
8. Brownell, W. E., C. R. Bader, and Y. de Ribaupierre. 1985. Evoked mechanical responses of isolated cochlear outer hair cells. *Science.* 227:194–196.
9. Dallos, P., X. Wu, and J. Zuo. 2008. Prestin-based outer hair cell motility is necessary for mammalian cochlear amplification. *Neuron.* 58:333–339.
10. Fisher, J. A. N., F. Nin, and A. J. Hudspeth. 2012. The spatial pattern of cochlear amplification. *Neuron.* 76:989–997.
11. Martin, P., D. Bozovic, and A. J. Hudspeth. 2003. Spontaneous oscillation by hair bundles of the bullfrog's sacculus. *J. Neurosci.* 23:4533–4548.
12. Ó Maoiléidigh, D., E. M. Nicola, and A. J. Hudspeth. 2012. The diverse effects of mechanical loading on active hair bundles. *Proc. Natl. Acad. Sci. USA.* 109:1943–1948.
13. Salvi, J. D., D. Ó Maoiléidigh, and A. J. Hudspeth. 2016. Identification of bifurcations from observations of noisy biological oscillators. *Biophys. J.* 111:798–812.
14. Tinevez, J.-Y., F. Jülicher, and P. Martin. 2007. Unifying the various incarnations of active hair-bundle motility by the vertebrate hair cell. *Biophys. J.* 93:4053–4067.
15. Salvi, J. D., D. Ó Maoiléidigh, and A. J. Hudspeth. 2015. Control of a hair bundle's mechanosensory function by its mechanical load. *Proc. Natl. Acad. Sci. USA.* 112:E1000–E1009.
16. Ó Maoiléidigh, D., and A. J. Hudspeth. 2018. Sinusoidal-signal detection by active, noisy oscillators on the brink of self-oscillation. *Physica D.* 378–379:33–45.
17. Risler, T., J. Prost, and F. Jülicher. 2004. Universal critical behavior of noisy coupled oscillators. *Phys. Rev. Lett.* 93:175702.
18. Dierkes, K., B. Lindner, and F. Jülicher. 2008. Enhancement of sensitivity gain and frequency tuning by coupling of active hair bundles. *Proc. Natl. Acad. Sci. USA.* 105:18669–18674.
19. Prakash, R., and A. J. Ricci. 2008. Hair bundles teaming up to tune the mammalian cochlea. *Proc. Natl. Acad. Sci. USA.* 105:18651–18652.
20. Pikovsky, A., M. Rosenblum, and J. Kurths. 2001. Synchronization: A Universal Concept in Nonlinear Sciences. Cambridge University Press, Cambridge, UK.
21. Acebrón, J. A., L. L. Bonilla, …, R. Spigler. 2005. The Kuramoto model: a simple paradigm for synchronization phenomena. *Rev. Mod. Phys.* 77:137–185.
22. Ahn, K.-H. 2013. Enhanced signal-to-noise ratios in frog hearing can be achieved through amplitude death. *J. R. Soc. Interface.* 10:20130525.
23. Kim, K.-J., and K.-H. Ahn. 2014. Amplitude death of coupled hair bundles with stochastic channel noise. *Phys. Rev. E Stat. Nonlin. Soft Matter Phys.* 89:042703.
24. Dierkes, K., F. Jülicher, and B. Lindner. 2012. A mean-field approach to elastically coupled hair bundles. *Eur Phys J E Soft Matter.* 35:37.
25. Gomez, F., T. Lorimer, and R. Stoop. 2016. Signal-coupled subthreshold Hopf-type systems show a sharpened collective response. *Phys. Rev. Lett.* 116:108101.
26. Ji, S., D. Bozovic, and R. Bruinsma. 2018. Amphibian sacculus and the forced Kuramoto model with intrinsic noise and frequency dispersion. *Phys. Rev. E.* 97:042411.
27. Barral, J., K. Dierkes, …, P. Martin. 2010. Coupling a sensory hair-cell bundle to cyber clones enhances nonlinear amplification. *Proc. Natl. Acad. Sci. USA.* 107:8079–8084.
28. Zhang, T.-Y., S. Ji, and D. Bozovic. 2015. Synchronization of spontaneous active motility of hair cell bundles. *PLoS One.* 10:e0141764.
29. Hartigan, J. A., and P. M. Hartigan. 1985. The dip test of unimodality. *Ann. Stat.* 13:70–84.
30. Aronson, D. G., G. B. Ermentrout, and N. Kopell. 1990. Amplitude response of coupled oscillators. *Physica D.* 41:403–449.
31. Koseska, A., E. Volkov, and J. Kurths. 2013. Oscillation quenching mechanisms: amplitude vs. oscillation death. *Phys. Rep.* 531:173–199.
32. Roongthumskul, Y., and D. Bozovic. 2015. Mechanical amplification exhibited by quiescent saccular hair bundles. *Biophys. J.* 108:53–61.
33. Roongthumskul, Y., L. Fredrickson-Hemsing, and D. Bozovic. 2011. Multiple-timescale dynamics underlying spontaneous oscillations of saccular hair bundles. *Biophys. J.* 101:603–610.
34. Faber, J., and D. Bozovic. 2019. Chaotic dynamics enhance the sensitivity of inner ear hair cells. *Sci. Rep.* 9:18394.
35. Nadrowski, B., P. Martin, and F. Jülicher. 2004. Active hair-bundle motility harnesses noise to operate near an optimum of mechanosensitivity. *Proc. Natl. Acad. Sci. USA.* 101:12195–12200.
36. Landau, L. D., and E. M. Lifshitz. 1986. Theory of Elasticity. Butterworth-Heinemann, Oxford, UK.
37. Barral, J., F. Jülicher, and P. Martin. 2018. Friction from transduction channels' gating affects spontaneous hair-bundle oscillations. *Biophys. J.* 114:425–436.
38. Bormuth, V., J. Barral, and P. Martin. 2014. Transduction channels' gating can control friction on vibrating hair-cell bundles in the ear. *Proc. Natl. Acad. Sci. USA.* 111:7185–7190.